JACS
JOURNAL OF THE AMERICAN CHEMICAL SOCIETY
pubs.acs.org/JACS
Article

Origin of Selectivity in Alternating Current-Enabled Partial Reduction of (Hetero)Arenes: A Case Study of Two Consecutive Irreversible Electrochemical Steps

Sreesaila Sreekumar, Joshua A. Beeler, Diptangshu Datta Mal, Henry S. White, and Long Luo*

Cite This: https://doi.org/10.1021/jacs.5c08873
Read Online

ABSTRACT: Herein, we investigate the origin of selectivity in the alternating current (AC)-enabled partial reduction of (hetero)arenes to cyclic alkenes. Reduction of (hetero)arenes can be considered as a reaction involving two consecutive irreversible electrochemical steps: the first generates the desired cyclic alkene, while the second leads to its undesired overreduction. Conventional constant current or voltage (DC) electrolysis results in poor selectivity toward the partial reduction products, originating from overreduction and base-induced decomposition of the desired product. Fast-scan cyclic voltammetry shows that the rate constant for the first reduction (k_1) exceeds that of the second one (k_2). Finite element simulations based on this experimental finding semiquantitatively capture the frequency-dependent selectivity observed in AC electrolysis experiments (i.e., increasing the AC frequency enhances selectivity). The results further reveal that AC electrolysis mitigates the low selectivity by only collecting the products at the initial stage of the reduction reaction, which is mostly under a kinetically controlled regime. We then extend the finite element model and introduce ΔE_{FOW}, the foot-of-the-wave potential difference between cyclic voltammograms of substrate and partial reduction product, as an accessible proxy for k_2/k_1. A ΔE_{FOW} > 80 mV predicts synthetically useful selectivity (>30%) toward the partial reduction product below 100 Hz.

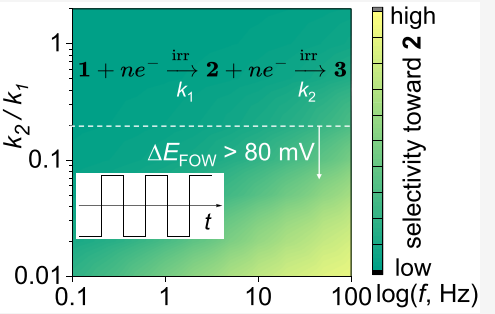

INTRODUCTION

Alternating current (AC) electrolysis is emerging as a powerful electrosynthesis strategy for achieving unique reactivities by introducing a temporal dimension through the periodic modulation of voltage or current. Recent advances have shown that AC electrolysis can overcome key limitations of DC electrolysis across a range of organic reactions. For example, Hilt's group used AC to prevent overoxidation or over-reduction in sulfur−sulfur bond metathesis and to enable the acyl nitroso Diels−Alder reaction.[1,2] Luo's group leveraged AC frequency optimization for selective amine functionalization,[3] improving redox-labile group tolerance,[4] and selective deuterium labeling.[5] Semenov's group improved the yield and scalability of Ni-catalyzed reactions using AC,[6,7] while Lei's group addressed metal catalyst deposition issues and developed various C−H functionalization methods.[8−12] Baran's group introduced AC-enabled chemoselective reductions,[13,14] Kolbe reactions,[15] and decarboxylative couplings.[16] Meanwhile, Hibino's group demonstrated AC-enabled methane-to-methanol conversion,[17] and He's group applied pulse electrolysis for cascade reactions.[18] Other applications include AC-promoted denitrative cyclizations,[19] selective hydrocarboxylations of olefins,[20] and enhanced control in electrochemically mediated polymerizations.[21]

Despite these successes in AC-enabled reaction discovery, the mechanistic understanding of these reactivities remains limited due to the inherent complexity of AC-driven processes. Thus, developing a comprehensive and quantitative understanding of how AC electrolysis enhances reaction outcomes is crucial. Such insights would enable the rational design of new AC reactions and the prediction of optimal reaction conditions, moving beyond conventional trial-and-error approaches.

Efforts are being made to address this gap. For example, the Luo group has investigated how AC electrolysis influences reaction outcomes following an Electrochemical−Chemical−Electrochemical (ECE) sequence, using alkyl amine oxidation as a model system and cyclic voltammetry (CV) as a key analytical tool.[3] By analyzing scan-rate-dependent CV features, an accurate prediction of the optimal AC frequency for selective amine arylation was achieved. In parallel, Yuen-Zhou and co-workers developed a theoretical framework to predict the outcomes of two competing reversible electrochemical reactions under AC electrolysis, both with and without stirring effects.[22,23] This theoretical model was successfully applied to

Received: May 26, 2025
Revised: July 9, 2025
Accepted: July 15, 2025

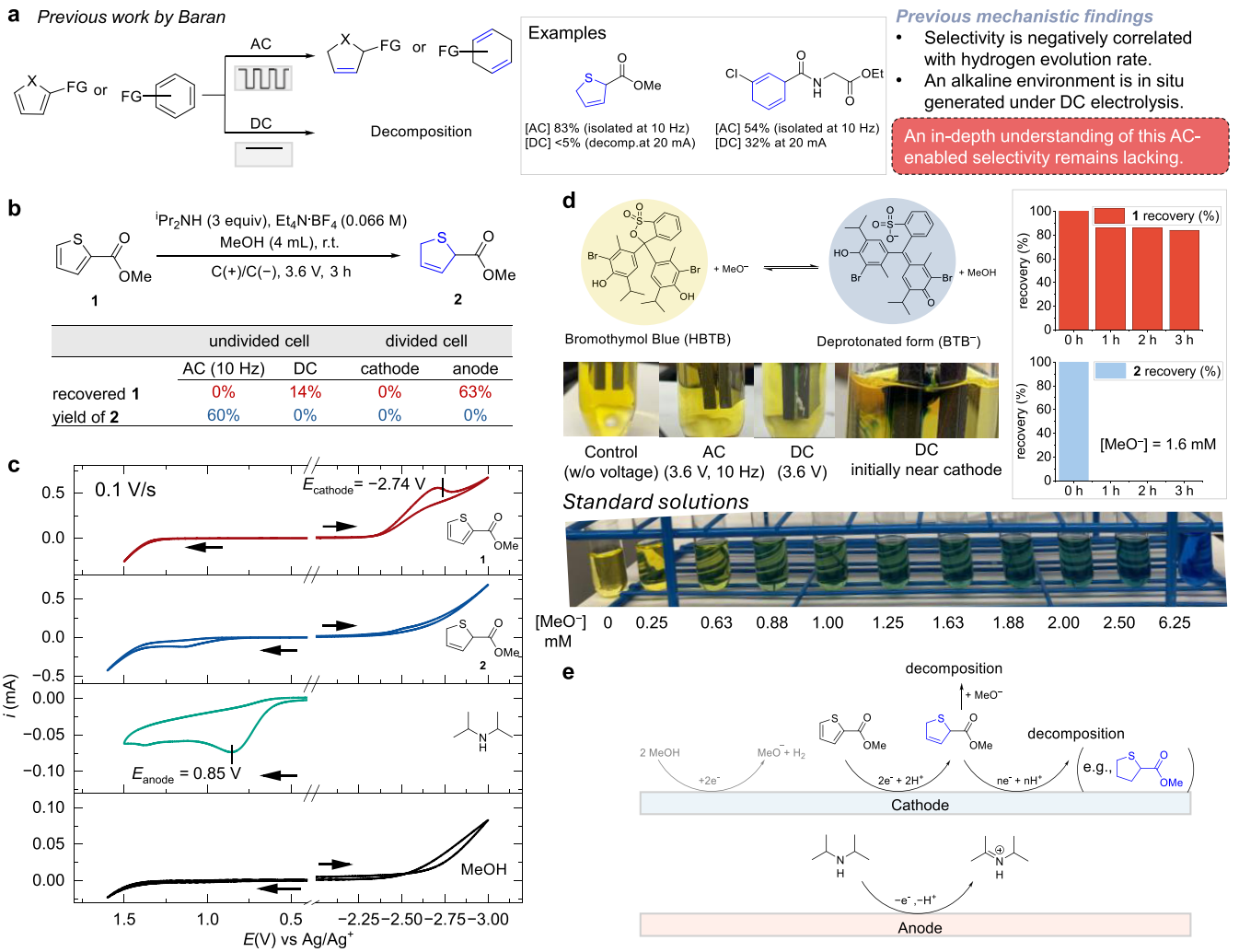

Figure 1. (a) Summary of the previous work by Baran and co-workers on AC-enabled selective partial reduction of (hetero)arenes. (b) Product comparison for **1** reduction between AC electrolysis using a 10 Hz square waveform (amplitude: 3.6 V) and DC electrolysis performed in both divided and undivided cells at 3.6 V, consisting of two glassy carbon plate electrodes. (c) Cyclic voltammograms (CVs) of compounds **1**, **2**, $^{i}Pr_2NH$, and MeOH at 0.1 V/s. Arrows indicate the initial scan direction. The working electrode is a 3 mm diameter glassy carbon disk electrode, the reference electrode is a freshly prepared Ag/10 mM Ag^+ reference electrode, the counter electrode is a Pt wire electrode, and the electrolyte is 0.066 M TEA·BF_4 in MeOH. (d) MeO^- concentration measurements using bromothymol blue as an indicator. The photographs show the solution colors in the presence of the indicator without applying a voltage bias, under AC and DC, as well as a series of standard solutions with different concentrations of MeO^-. The bar graphs in the box show the recovery of **1** and **2** during the stability test in the presence of 1.6 mM MeO^-. (e) Schematic illustration of the decomposition pathways of **1** during DC electrolysis.

describe experimentally obtained yields and branching ratios during the reduction of acetophenone.

This work aims to uncover the origin of AC-enabled selectivity for reactions involving two consecutive irreversible electrochemical steps. We used AC-enabled partial reduction of (hetero)arenes to cyclic alkenes as our model reaction. Partial hydrogenation of (hetero)arenes offers a direct route to unsaturated cyclic compounds and is widely employed in the synthesis of pharmaceuticals, polymer intermediates, and food products.[12,14,24,25] However, conventional hydrogenation methods typically require harsh conditions to disrupt aromaticity, often compromising selectivity. The AC-enabled partial reduction of (hetero)arenes under mild reaction conditions was originally discovered by Baran and co-workers.[14] During reaction development, they observed that DC electrolysis of (hetero)arene starting materials resulted in nearly complete decomposition or partial recovery. In contrast, AC electrolysis at 10 Hz gave moderate to good yields of the desired cyclic alkene products (Figure 1a). Based on empirical observations that hydrogen gas formation is suppressed under AC compared to DC, they proposed that the change in selectivity might arise from competition between the hydrogen evolution reaction and (hetero)arene reduction. Additionally, the base generated during hydrogen evolution was believed to promote further undesired side reactions, compounding the selectivity differences between AC and DC electrolysis. However, an in-depth and quantitative understanding of this AC-enabled selectivity remains lacking. Key questions—such as how selectivity depends on AC frequency and how this relationship can be generalized to other reactions with similar mechanistic features—remain unanswered. Addressing these questions is critical for the rational design of future AC-enabled reactions.

https://doi.org/10.1021/jacs.5c08873
J. Am. Chem. Soc. XXXX, XXX, XXX−XXX

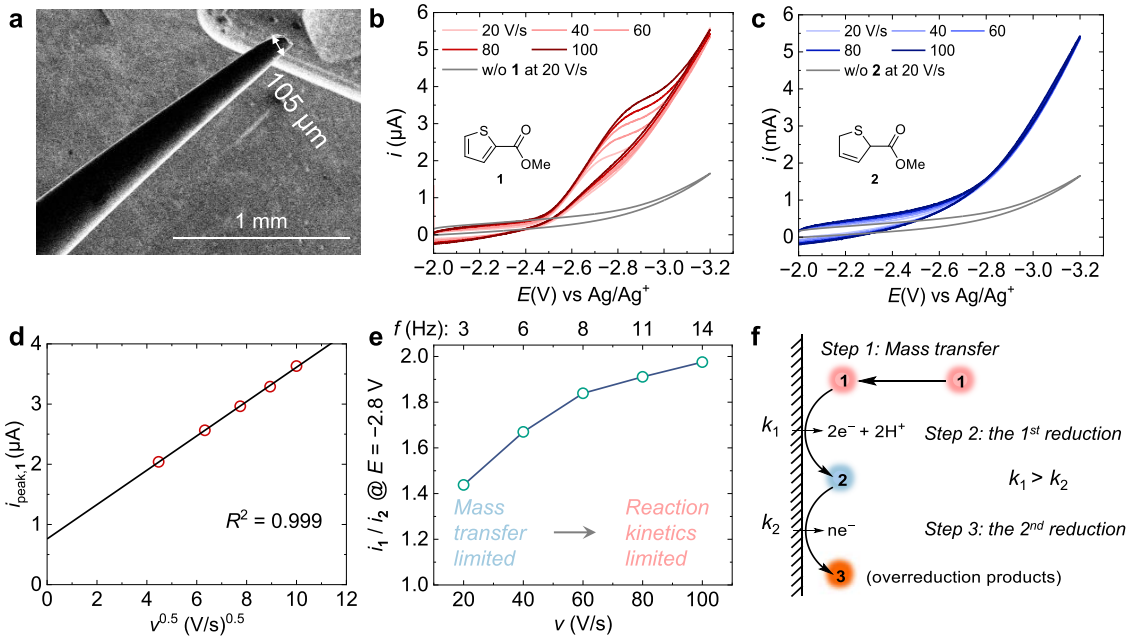

Figure 2. Fast-scan cyclic voltammetry study. (a) Scanning electron micrograph of a carbon microfiber disk electrode used for the fast-scan voltammetric measurements. (b, c) CVs of (b) 5 mM **1** and (c) 5 mM **2** in a MeOH solution containing 0.066 M TEA·BF_4, recorded at scan rates ranging from 20 to 100 V/s. Gray curves represent background CVs without **1** or **2** at 20 V/s. (d) Plot of peak currents in panel b ($i_{peak,1}$) vs the square root of scan rate ($v^{0.5}$). Experimental values are denoted by open red circles, and the black line is a linear fit of the experimental data with an R^2 value of 0.999. (e) Plot of the current ratio for **1** and **2** reduction (i_1/i_2) at −2.8 V in panels b and c as a function of scan rate (v) and its equivalent AC frequency (f). The v-to-f conversion is detailed in the SI. (f) Schematic illustration of the reaction steps.

RESULTS AND DISCUSSION

Understanding the Poor Performance under DC Electrolysis. Figure 1b shows the reaction outcomes for the reduction of methyl thiophene-2-carboxylate, **1**, under AC electrolysis using a 10 Hz square waveform (amplitude: 3.6 V) and DC electrolysis in both divided and undivided cells at 3.6 V. Consistent with Baran's findings, DC electrolysis in an undivided cell produces no detectable partial reduction product, **2**, and recovers only ∼ 14% of unreacted **1**. In contrast, AC electrolysis affords a 60% yield of **2**. The results from the divided cell indicate that the decomposition of **1** predominantly occurs at the cathode rather than the anode. The experimental setups are shown in Figures S1 and S2. Gas chromatography−mass spectrometric (GC-MS) analysis of the reaction mixture in the cathodic compartment shows the formation of tetrahydrothiophene-2-carboxylate, a hydrogenation product of **2** (Figure S2d).

These synthetic results align with the CV data presented in Figure 1c, which show that both **1** and **2** can be reduced at a cell voltage of 3.6 V (cathode potential ∼ −2.74 V vs Ag/Ag^+, Figure S2), and the anodic current is primarily due to the oxidation of $^iPr_2NH$ (anode potential ∼ +0.85 V vs Ag/Ag^+).

Additionally, the CV in Figure 1c suggests that MeOH reduction should occur at the cathode under DC electrolysis conditions. To quantify the extent of MeOH reduction, we estimated the concentration of MeO^- generated under both AC and DC conditions using bromothymol blue (HBTB) as a colorimetric indicator.

Figure 1d shows photographs of the reaction solutions after 10 min of electrolysis with a 3.6 V 10 Hz AC bias and with a 3.6 V DC bias, as well as in the absence of a voltage bias, alongside a series of standard solutions containing 0 to 6.25 mM MeO^- (see details in the SI). The color transition from yellow to green to blue is due to increasing MeO^- concentration, which shifts HBTB to its deprotonated form, BTB^-. UV−vis absorption measurements reveal a linear relationship between peak absorbance intensity at ∼ 420 nm and [MeO^-] up to 1.6 mM (Figure S9). Based on UV−vis absorbance, [MeO^-] was estimated to be >1.6 mM for the DC electrolysis solution and ∼ 0.5 mM for the AC electrolysis solution. To assess the stability of compounds **1** and **2** under basic conditions, both were exposed to 1.6 mM MeO^- for 1 to 3 h. After 3 h, ∼ 80% of **1** remained, whereas **2** completely decomposed within 1 h (Figure S10). Taken together, these results suggest that the lack of **1**-to-**2** conversion under DC conditions can be attributed to both the direct electrochemical overreduction of **2** and the base-catalyzed chemical decomposition of **2** (Figure 1e).

Fast-Scan Voltammetric Study. Next, we employed fast-scan voltammetry to investigate the electrochemical behavior of **1** and **2** at a time scale comparable to an AC electrolysis pulse (10 Hz, or ∼100 ms), to understand the improved selectivity toward **2** under AC conditions. The equivalent scan rate for 10 Hz was calculated to be ∼ 72 V/s (Figure S8). At such high scan rates, background charging currents distort the voltammetric features of **1** and **2** when using a conventional millimeter-sized glassy carbon electrode (Figure S6).

To address this issue, we fabricated a ∼105 μm diameter carbon microdisk electrode from carbon fibers (Figure 2a). The microelectrode substantially reduced contributions to the current from electrical double-layer capacitance and iR drop, thereby enabling unobscured measurement of faradaic currents at scan rates of several hundred volts per second.[26,27] Details on microelectrode fabrication and electrochemical characterization are provided in Figure S11.

Figure 2b,c show CVs of 5 mM **1** and 5 mM **2** in a MeOH solution containing 0.066 M TEA·BF_4 recorded at scan rates ranging from 20 to 100 V/s. Gray curves represent background

https://doi.org/10.1021/jacs.5c08873
J. Am. Chem. Soc. XXXX, XXX, XXX−XXX

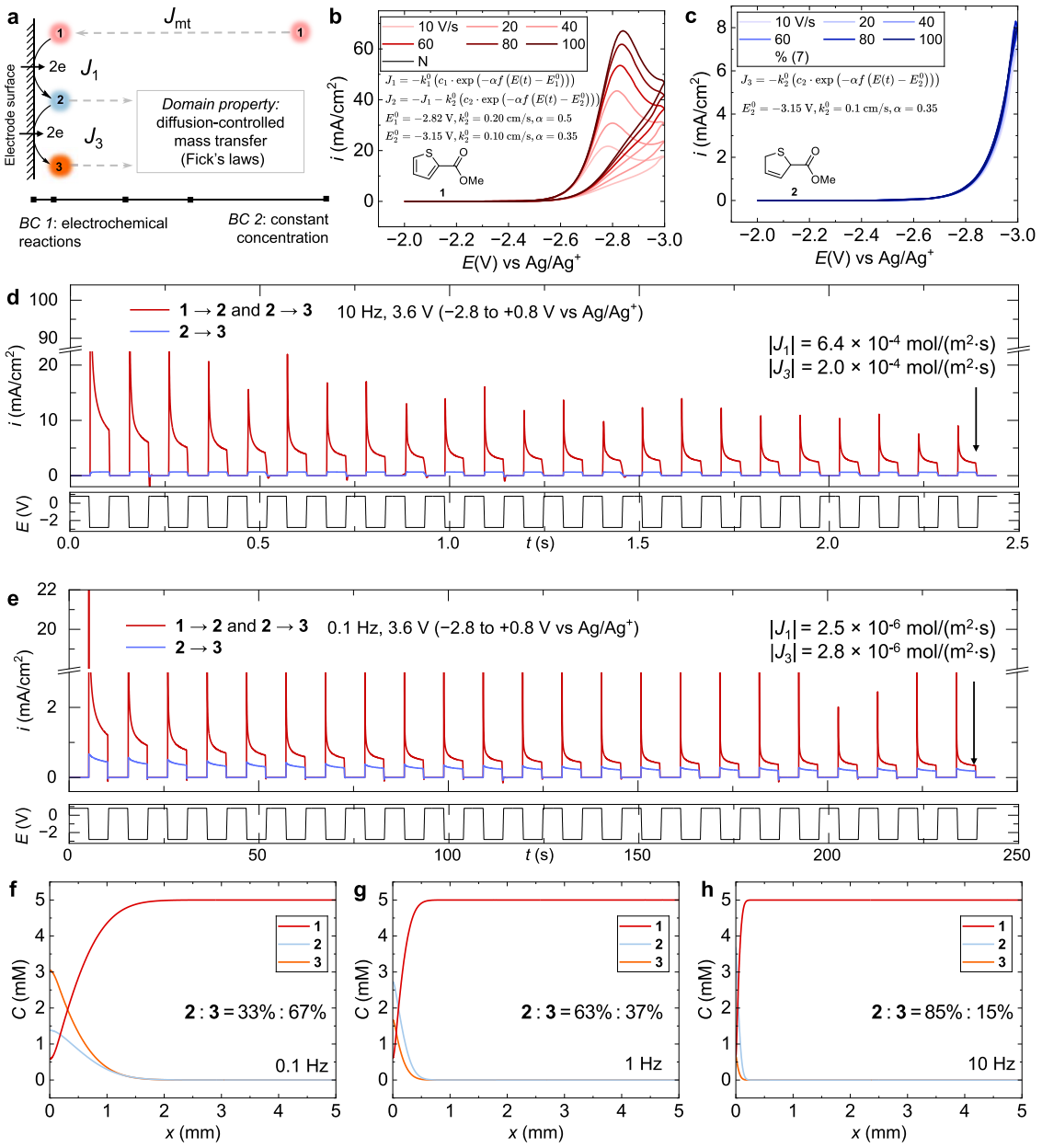

Figure 3. Finite element simulation. (a) One-dimensional geometry, boundary conditions (BC), and domain properties of the model. The electroreduction of **1** is simplified as two consecutive two-electron electrochemical reduction steps: **1** + 2e → **2** and **2** + 2e → **3**. Note that **3** is a hypothetical overreduction product analogous to experimentally observed overreduction and degradation products. In the experiment, **2** can undergo multiple reduction steps involving multiple electrons. J_{mt} is the mass transfer flux of **1** from the bulk solution to the electrode surface, J_1 is the electrochemical reaction flux of **1** at the electrode surface, and J_3 is the flux of **3** generated at the electrode surface which is also equal to the flux of **2** consumed at the electrode surface. (b, c) Simulated CVs for (b) 5 mM **1** and (c) 5 mM **2** at scan rates between 10 and 100 V/s. The electrochemical reaction kinetics for **1** and **2** are described by the Tafel equation with parameters provided in the inset. J_2 is the flux of **2** at the electrode surface, which is equal to the difference between the influx from **1** reduction and outflux from **2** reduction. (d, e) Simulated total current for **1** → **2** → **3** and specific current for **2** → **3** at (d) 10 Hz and (e) 0.1 Hz with an upper and lower amplitude of +0.8 and −2.8 V vs Ag/Ag$^+$, respectively. (f–h) Simulated concentration profiles for **1**, **2**, and **3** at the end of the simulation at (f) 0.1 Hz, (g) 1 Hz, and (h) 10 Hz. The insets show the ratio of the total amounts of **2** and **3** produced for each AC frequency.

CVs recorded without **1** or **2** at 20 V/s (i.e., only the supporting electrolyte solution of 0.066 M TEA·BF$_4$ in MeOH). The reduction current for **1** begins to increase near −2.5 V vs Ag/Ag$^+$ and reaches a peak between −2.7 and −2.8 V. The peak current values ($i_{peak,1}$) scale linearly with the square root of the scan rate ($\nu^{0.5}$, Figure 2d), a characteristic feature of a diffusion-limited process, suggesting that the reduction of **1** is mass transfer-limited. In contrast, the reduction current for **2** shows no noticeable scan rate dependence and lacks a distinct voltammetric peak, indicating that its reduction is limited by electron-transfer kinetics rather than by mass transfer. Comparison of both sets of voltammograms shows that the electron-transfer kinetics of **1** are faster than for **2** (i.e., $k_1 > k_2$, Figure 2f). During AC electrolysis, the potential switches back and forth between +0.8 and −2.8 V, which is analogous to scanning in the same potential window in a CV experiment. Thus, the current ratio for the reduction of **1** and **2** (i_1/i_2) at −2.8 V can be used as a descriptor of

https://doi.org/10.1021/jacs.5c08873
J. Am. Chem. Soc. XXXX, XXX, XXX−XXX

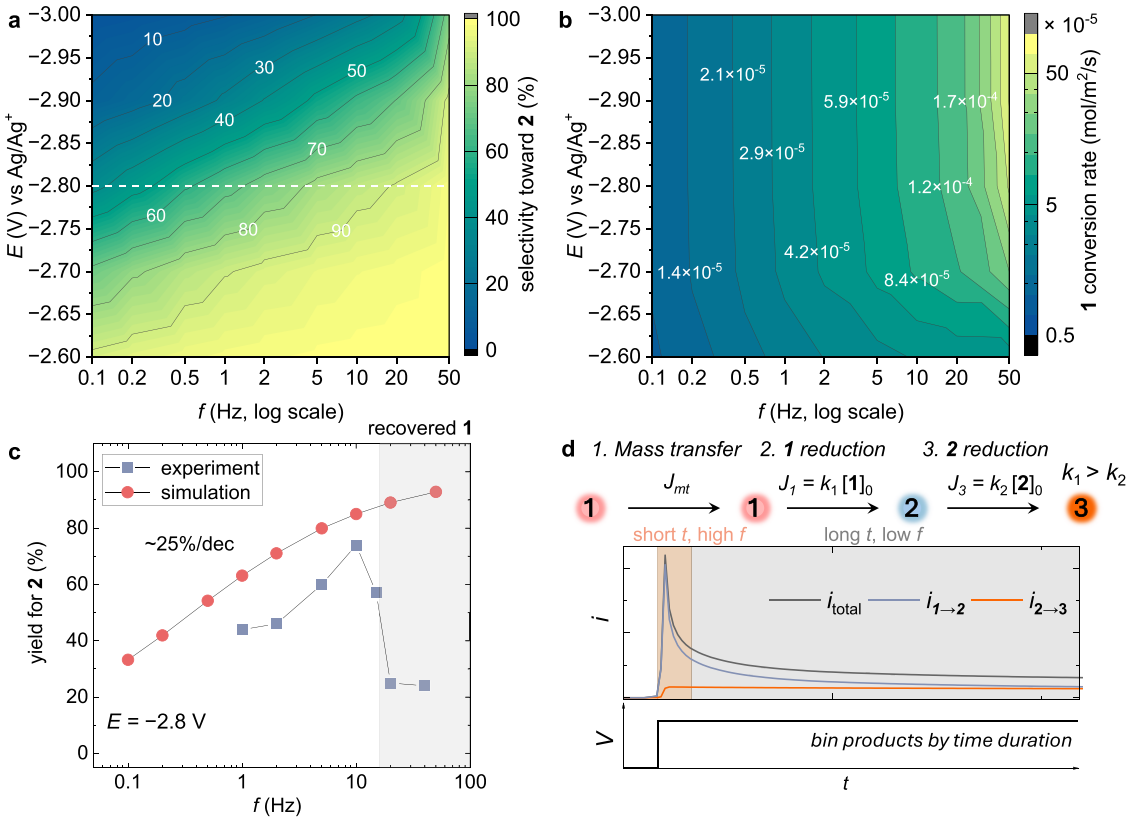

Figure 4. (a, b) Contour plots of (a) the simulated selectivity toward product **2** and (b) the **1** conversion rate as a function of f at the log scale and cathodic potential during AC electrolysis. (c) Comparison between experimental and simulated yield for **2** as a function of f at −2.8 V vs Ag/Ag^+. (d) Mechanism behind the AC-enabled selective partial reduction of **1** to **2**.

reaction selectivity toward **2**: a higher i_1/i_2 ratio indicates greater selectivity for **2** over the undesired overreduction and decomposition products. As shown in Figure 2e, selectivity gradually improves with increasing equivalent frequency from 3 to 14 Hz, consistent with synthetic results discussed later (see Figure 4c).

Finite Element Simulations. Based on the fast-scan voltammetry results, we developed a finite element simulation model to reproduce the experimentally observed AC frequency-dependent selectivity toward **2** during the reduction of **1**. In this model, the electroreduction of **1** is simplified as two consecutive, two-electron, irreversible electrochemical steps: **1** + 2e → **2** and **2** + 2e → **3** (Figure 3a). Here, **3** is a hypothetical overreduction product. In reality, **2** may undergo multiple reduction steps involving several electrons. For simplicity, we approximate all subsequent reductions of **2** and its intermediates as a single, hypothetical two-electron reduction step. The starting material, **1**, diffuses from the bulk solution (at x = 5 mm) to the electrode surface (x = 0 mm). The fluxes for the electrochemical reduction of **1** and **2** (J_1 and J_3, respectively) are described using the following Tafel equations

$$J_1 = -k_1^0(c_1 \cdot \exp\left(-\frac{\alpha F(E(t) - E_1^0)}{RT}\right)) \quad (1)$$

$$J_3 = -k_2^0(c_2 \cdot \exp\left(-\frac{\alpha F(E(t) - E_2^0)}{RT}\right)) \quad (2)$$

where k_1^0 and k_2^0 are the standard heterogeneous electron transfer rate constants, $c_1$and c_2 are the concentrations of **1** and **2** at the electrode surface, α is the charge transfer coefficient, F is the Faraday's constant (96,480 C/mol), R is the ideal gas constant (8.314 J/mol·K), T is 298 K, and E_1^0 and E_2^0 are the standard reduction potentials for **1** and **2.**

Guided by the reported parameter ranges, we adjusted the values of k_1^0, k_2^0, E_1^0, and E_2^0 to reproduce the key features of the experimental CVs described earlier (see SI for the details regarding the value selection). A representative parameter set of k_1^0 = 0.2 cm/s, k_2^0 = 0.1 cm/s, E_1^0 = −2.82 V, and E_2^0 = −3.15 V yields simulated CVs in reasonable agreement with the experimental data (Figure 3b,3c). These parameters are phenomenological due to a lack of thermodynamic, kinetic, and mechanistic data. However, as evidenced by the fact that minor inaccuracies in k^0 can be offset by corresponding shifts in E^0 and the simulated CVs capture the key electrochemical features of the system (see Section 8 in the SI for detailed discussion) such that the overall conclusions of the simulation are unchanged. These parameters were used as inputs for the finite element model in COMSOL Multiphysics (modeling details are presented in the SI). A square-wave voltage profile ranging from +0.8 V to −2.8 V vs Ag/Ag^+ was applied across experimentally relevant frequencies. Notably, in the experiment, the sacrificial reagent ^{i}Pr$_2$NH is oxidized during the anodic phase but does not participate in the reduction of either **1** or **2**; thus, no anodic reaction was considered in this model during the positive phase of the AC waveform.

Figure 3d shows the simulated total current density for the sequential reductions of **1** → **2** and **2** → **3** (i_{total}, red curve), along with the specific current associated with the over-

https://doi.org/10.1021/jacs.5c08873
J. Am. Chem. Soc. XXXX, XXX, XXX−XXX

reduction of **2** to **3** at 10 Hz ($i_{overred}$, blue curve). The ratio $i_{total}/i_{overred}$ indicates selectivity toward **2** where a larger ratio corresponds to higher selectivity. During each cathodic pulse, i_{total} exhibits a rapid decay due to depletion of **1** near the electrode surface over time (Figure S13a,c). Meanwhile, a small portion of **2** is converted to **3** at a relatively slow but stable rate (Figure S13b). During the following anodic pulse, the concentration of **1** near the electrode partially recovers through diffusion from bulk solution (Figure S13d). In the next cycle, i_{total} decreases further due to the lower local concentration of **1**. This decline continues for 6−7 AC cycles (Figure 3d), until the consumption rate of **1** during the cathodic pulse becomes comparable to its replenishment rate during the anodic pulse. At this point, the system reaches a dynamic steady state with preferential generation of **2** over **3**, as evidenced by the magnitude of J_1 being more than three times greater than that of J_3 at the end of the cathodic pulse (6.4×10^{-4} vs 2.0×10^{-4} mol/m^2·s).

The same calculation was performed for 1.0 and 0.1 Hz, using the same AC amplitude of 3.6 V. Figure 3e displays the current vs time plot for 0.1 Hz. Similarly, i_{total} first declines and then reaches a dynamic steady state. However, i_{total} is significantly lower than its counterpart at 10 Hz due to the expanded diffusion layer for **1** (∼ 1 mm when f = 0.1 Hz compared to ∼ 0.2 mm when f = 10 Hz, Figure 3e), which limits the mass transfer rate of **1** to the electrode surface. The $i_{total}/i_{overred}$ ratio is ∼ 2:1, meaning a majority of **2** undergoes overreduction to **3**. This finding is further supported by the similar values of J_1 and J_3 at the end of the cathodic pulse (2.5×10^{-6} vs 2.8×10^{-6} mol/m^2·s).

The simulated concentration profiles of **1**, **2**, and **3** at the end of each simulation (Figures 3f−h) clearly show that increasing f corresponds to a decrease in diffusion layer thickness and improved selectivity toward **2**. Integration of the concentration profiles provides an estimate of the theoretical selectivity toward **2** and **3**: 33%/67% at 0.1 Hz, 63%/37% at 1 Hz, and 85%/15% at 10 Hz. The selectivity result remains unchanged with different initial concentrations of **1** (Figure S14) and is relatively unchanged throughout the reaction (Figure S15).

We further evaluated the theoretical selectivity toward **2** across a two-dimensional parameter space defined by f and cathode potential ($E_{cathode}$) (Figure 4a). The analysis reveals that increasing f or decreasing $E_{cathode}$ enhances selectivity toward **2**, as both adjustments shift the reduction steps into a kinetically controlled regime for the reduction of **1** such that the **1** → **2** transformation is favored over the overreduction of **2** → **3**. However, a key limitation of tuning the selectivity by decreasing $E_{cathode}$ is the concomitant slowdown in **1** conversion, leading to extended reaction times (Figure 4b). For example, at −2.65 V and f = 0.5 Hz, ∼ 90% selectivity for **2** is achieved, a value comparable to that obtained at −2.8 V with f = 20 Hz. However, the conversion rate of **1** when $E_{cathode}$ = −2.65 V is approximately 10-fold lower than that at −2.8 V (1.7×10^{-5} vs 1.4×10^{-4} mol·m^{-2}·s^{-1}). These results underscore the importance of balancing product selectivity with reaction efficiency in optimizing AC electrolysis conditions.

Finally, we compared our theoretical predictions with experimental results at 3.6 V as a function of f. As shown in Figure 4c, the predicted yield of **2** exhibits an approximately 25% per decade increase with log(f), closely matching the experimental trend observed from 1 to 10 Hz. However, two notable discrepancies are observed. First, the predicted yields are slightly higher than the experimental values. This difference may arise from the simulation's assumption of a semi-infinite boundary condition—that is, the bulk concentration of **1** is held constant. In practice, as the reaction proceeds, the bulk concentration of **1** decreases while **2** accumulates, increasing the likelihood of overreduction of **2** to **3**. This accumulation effect decreases the overall selectivity toward **2** at full conversion, thereby accounting for the lower experimental yields. Second, at frequencies >10 Hz, the simulation predicts further increases in the yield of **2**, while the experimental yield of **2** decreases. This decline may be attributed to the voltage losses caused by charging and discharging of the electric double layer at f > 20 Hz (Figure S5). Consistent with this interpretation, a noticeable amount of unreacted **1** was recovered under these conditions.

Generalization of Theoretical Findings. The results and discussion presented above clearly demonstrate that the AC-enabled selective partial reduction of **1** is governed by two key factors: (i) the suppression of MeO^- accumulation that leads to the strong base (like MeO^-)-induced chemical decomposition of **2**, observed under DC electrolysis conditions (Figure 1d), and (ii) the modulation of mass transfer of **1**, which shifts the system into a kinetically controlled regime, thereby enhancing selectivity toward **2**.

The first factor is specific to the protic solvent employed in this reaction. In contrast, the second factor is anticipated to be generalizable to chemical systems involving two consecutive irreversible electrochemical steps, where the first step is kinetically facile relative to the second (i.e., $k_1 > k_2$). Figure 4d schematically illustrates this second effect by showing the time-dependent evolution of the total current (i_{total}) and the specific currents for **1** to **2** and **2** to **3** conversions ($i_{1\to2}$ and $i_{2\to3}$). Upon applying the cathodic pulse, species **1** is rapidly converted to **2**. Since $k_1 > k_2$, the subsequent conversion of **2** to **3** initially lags behind, and i_{total} is dominated by $i_{1\to2}$. However, as the pulse duration increases, the conversion of **2** to **3** catches up, $i_{1\to2}$ becomes comparable to $i_{2\to3}$, leading to complete overreduction to **3**.

At different f, we are effectively binning the products over different time intervals, thereby controlling the product distribution.

The difference between k_1 and k_2 arises from the disparities in the standard reduction potentials (E^0), the standard electron transfer rate constants (k^0), or both, as described by the following expressions derived from eqs 1 and 2

$$k_1 = -k_1^0 \exp\left(-\frac{\alpha F(E(t) - E_1^0)}{RT}\right) \quad (3)$$

$$k_2 = -k_2^0 \exp\left(-\frac{\alpha F(E(t) - E_2^0)}{RT}\right) \quad (4)$$

To generalize our findings and provide guidance for future reaction design, we modified the finite element simulation model to evaluate the dependence of selectivity toward **2** on the k_2/k_1 ratio and f. As previously discussed, selectivity is influenced by the applied potential. Since the peak potential is most readily identified experimentally, we chose −2.8 V as the working potential in the simulations. We also fixed α at 0.5 for both electrochemical steps, as this is the most common value. Subsequently, k_1^0 and k_2^0 were varied to generate different k_2/k_1 ratios for analysis.

https://doi.org/10.1021/jacs.5c08873
J. Am. Chem. Soc. XXXX, XXX, XXX−XXX

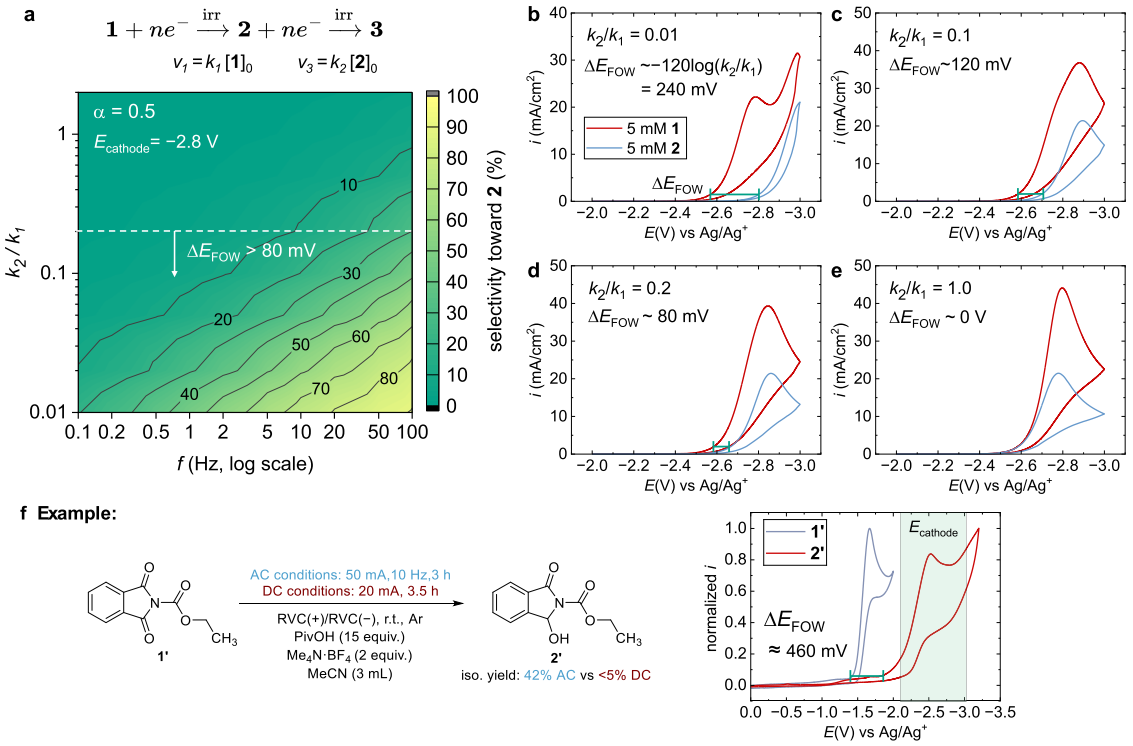

Figure 5. Generalization of theoretical predictions. (a) Simulated selectivity toward **2** as a function of f and the ratio of the rate constants (k_1 and k_2) for two consecutive irreversible electrochemical reactions. The electrochemical kinetics are described by the Tafel equation with $\alpha = 0.5$. (b–e) Simulated CVs for 5 mM **1** (red) and 5 mM **2** (blue) at k_2/k_1 ratios ranging from 0.01 to 1.0. ΔE_{FOW} represents the potential difference at the foot of the wave (FOW) between the CVs of **1** and **2**. Only when ΔE_{FOW} > 80 mV (equivalent to k_2/k_1 < 0.2) can AC electrolysis achieve synthetically useful selectivity (>30%) toward **2** within a practical frequency range of ≤100 Hz. (f) Left: Electrochemical reduction of **1′** to **2′** under AC electrolysis conditions (50 mA, 10 Hz, 3 h) and DC electrolysis conditions (20 mA, 3.5 h). Right: CVs of **1′** and **2′** in the reaction mixture at 0.1 V/s showing $\Delta E_{FOW} \approx 460$ mV. The working electrode is a 3 mm diameter glassy carbon disk electrode, the reference electrode is a freshly prepared Ag/10 mM Ag^+ reference electrode, and the counter electrode is a Pt wire electrode. The mint green zone indicates the cathode potential window during DC electrolysis.

Figure 5a shows the simulated selectivity toward **2** as a function of f and the k_2/k_1 ratio for an electrochemical system involving two consecutive irreversible electrochemical steps. The contour plot reveals that decreasing the k_2/k_1 ratio or increasing f favors the formation of product **2**. Moreover, the effect of both parameters on selectivity appears nearly proportional, as indicated by the linearity of the contour curves.

To achieve a synthetically useful yield (>30%) of **2** within a practical frequency range (≤100 Hz), the k_2/k_1 ratio should not exceed 0.2. However, direct experimental determination of k_2/k_1 is often not trivial. To address this, we propose using the potential difference at the foot of the wave (FOW) between the CVs of **1** and **2** at equal concentrations, denoted as ΔE_{FOW}, as a proxy for the k_2/k_1 ratio. This rationale is based on the following derivation. In the FOW region, the reductions of **1** and **2** are governed by slow electrochemical kinetics. The faradaic current in the early stage of this region (i_1 and i_2) can be approximated as

$$i_1 = nFk_1^0 c_1^0 \exp\left(-\frac{\alpha F(E_1 - E_1^0)}{RT}\right) \quad (5)$$

$$i_2 = nFk_2^0 c_2^0 \exp\left(-\frac{\alpha F(E_2 - E_2^0)}{RT}\right) \quad (6)$$

where c_1^0 and c_2^0 are the bulk concentrations of **1** and **2**, respectively, and are equal. When $i_1 = i_2$, eqs 5 and (6) give,

$$nF{\cdot}k_1^0{\cdot}c_1^0{\cdot}\exp\left(-\frac{\alpha F(E_1 - E_1^0)}{RT}\right) = nF{\cdot}k_2^0{\cdot}c_2^0{\cdot}\exp\left(-\frac{\alpha F(E_2 - E_2^0)}{RT}\right)$$

Rearranging gives,

$$\exp\left(\frac{\alpha F(E_1 - E_2)}{RT}\right) = \left(\frac{k_1^0}{k_2^0}\right){\cdot}\exp\left(\frac{\alpha F(E_1^0 - E_2^0)}{RT}\right) = \frac{k_1}{k_2}$$

Therefore:

$$\Delta E_{FOW} = E_1 - E_2 = \frac{RT}{\alpha F}\ln\left(\frac{k_2}{k_1}\right) \approx 120\text{ mV} \times \log_{10}\left(\frac{k_2}{k_1}\right)$$

When k_2/k_1 < 0.2, $|\Delta E_{FOW}|$ > 80 mV. Simulated CVs for 5 mM **1** and **2** (Figure 5b–e) illustrate the ΔE_{FOW} values across various k_2/k_1 ratios. This leads to a useful rule of thumb: Only when $|\Delta E_{FOW}|$ > 80 mV (equivalent to k_2/k_1 < 0.2) AC electrolysis can achieve synthetically useful yield (>30%) toward an intermediate product within a practical frequency range (≤100 Hz).

To validate our rule, we tested another model reaction: the AC-enabled partial reduction of phthalimide (**1′**) to **2′**, previously reported by Baran and co-workers.[13] As shown in

https://doi.org/10.1021/jacs.5c08873
J. Am. Chem. Soc. XXXX, XXX, XXX−XXX

Figure 5f, no desired product **2′** was detected under constant current electrolysis at 20 mA for 3.5 h when **1′** was fully converted (with the cathode potential gradually increasing from −2.1 to −3.0 V during the reaction). This is consistent with the CV data for **2′**, which shows irreversible reduction beginning at $E_{cathode} < -1.9$ V. In contrast, we obtained a 42% yield of the desired product **2′** under AC electrolysis at a frequency of 10 Hz and a current amplitude of 50 mA for 3 h, even though $E_{cathode}$ is sufficiently negative to drive the reduction of **2′**. This experimental observation aligns with our rule of thumb, as there is a large $|\Delta E_{FOW}|$ (∼460 mV) between the CVs for the irreversible reduction of **1′** and **2′**.

CONCLUSIONS

In conclusion, we investigated the origin of selectivity in the AC-enabled partial reduction of (hetero)arenes to cyclic alkenes. Under DC electrolysis, both thiophene and its partially reduced cyclic alkene product undergo further electrochemical reduction, leading to undesired overreduction. Additionally, the accumulation of methoxide anions ($[MeO^-]$) under DC conditions promotes chemical decomposition of the alkene product.

Using fast-scan voltammetry, we found that the reduction of thiophene is primarily mass transfer-controlled, whereas the reduction of the cyclic alkene product is limited by slow electron-transfer kinetics, at the time scale relevant to AC electrolysis. By increasing AC frequency, the products in the initial stage of the cathodic pulse are sampled, where the product selectivity reflects the fast reaction kinetics for the first reduction, enhancing selectivity toward the partially reduced product. This mechanism is semiquantitatively validated through finite element simulations.

Our findings can be generalized to guide the design of AC-enabled selective transformations involving two consecutive irreversible electrochemical steps. A practical rule of thumb emerges: when $|\Delta E_{FOW}| > 80$ mV, AC electrolysis can achieve synthetically useful selectivity (>30%) toward the intermediate product within a practical frequency range (≤100 Hz).

ASSOCIATED CONTENT

Supporting Information

The Supporting Information is available free of charge at https://pubs.acs.org/doi/10.1021/jacs.5c08873.

General experimental details and instrumentation information, AC and DC electrolysis conditions, electroanalytical measurements, conversion between AC frequency and equivalent scan rates, measurement of electrogenerated methoxide, stability test for compounds **1** and **2**, preparation and sizing of microelectrodes, and COMSOL finite element simulation details (PDF)

CV for 1.mph (PDF)

CV for 2.mph (PDF)

AC waveform 10 Hz .mph (PDF)

AUTHOR INFORMATION

Corresponding Author

Long Luo − *Department of Chemistry, University of Utah, Salt Lake City, Utah 84112, United States;* orcid.org/0000-0001-5771-6892; Email: long.luo@utah.edu

Authors

Sreesaila Sreekumar − *Department of Chemistry, University of Utah, Salt Lake City, Utah 84112, United States*

Joshua A. Beeler − *Department of Chemistry, University of Utah, Salt Lake City, Utah 84112, United States;* orcid.org/0009-0001-9882-3173

Diptangshu Datta Mal − *Department of Chemistry, University of Utah, Salt Lake City, Utah 84112, United States;* orcid.org/0000-0001-7584-8848

Henry S. White − *Department of Chemistry, University of Utah, Salt Lake City, Utah 84112, United States*

Complete contact information is available at: https://pubs.acs.org/10.1021/jacs.5c08873

Author Contributions

The manuscript was written through the contributions of all authors.

Notes

The authors declare no competing financial interest.

ACKNOWLEDGMENTS

This work was primarily supported by NIH (1R35 GM142590). S.S. and L.L. also gratefully acknowledge support from the University of Utah, and the Alfred P. Sloan Foundation (Grant # FH-2023-20829). J. B. and H.S.W. are supported by the NSF Center for Synthetic Organic Electrochemistry, CHE-2002158. ChatGPT was used to improve the language and clarity of the manuscript during its preparation.

REFERENCES

(1) Sattler, L. E.; Otten, C. J.; Hilt, G. Alternating Current Electrolysis for the Electrocatalytic Synthesis of Mixed Disulfide via Sulfur-Sulfur Bond Metathesis towards Dynamic Disulfide Libraries. *Chem. - Eur. J.* **2020**, *26* (14), 3129−3136.

(2) Fährmann, J.; Hilt, G. Alternating Current Electrolysis as Efficient Tool for the Direct Electrochemical Oxidation of Hydroxamic Acids for Acyl Nitroso Diels-Alder Reactions. *Angew. Chem., Int. Ed.* **2021**, *60* (37), 20313−20317, DOI: 10.1002/anie.202107148.

(3) Gunasekera, D.; Mahajan, J. P.; Wanzi, Y.; Rodrigo, S.; Liu, W.; Tan, T.; Luo, L. Controlling One- or Two-Electron Oxidation for Selective Amine Functionalization by Alternating Current Frequency. *J. Am. Chem. Soc.* **2022**, *144* (22), 9874−9882.

(4) Rodrigo, S.; Hazra, A.; Mahajan, J. P.; Nguyen, H. M.; Luo, L. Overcoming the Potential Window-Limited Functional Group Compatibility by Alternating Current Electrolysis. *J. Am. Chem. Soc.* **2023**, *145* (40), 21851−21859.

(5) Behera, N.; Gunasekera, D.; Mahajan, J. P.; Frimpong, J.; Liu, Z. F.; Luo, L. Electrochemical Hydrogen Isotope Exchange of Amines Controlled by Alternating Current Frequency. *Faraday Discuss.* **2023**, *247* (0), 45−58.

(6) Bortnikov, E. O.; Semenov, S. N. Coupling of Alternating Current to Transition-Metal Catalysis: Examples of Nickel-Catalyzed Cross-Coupling. *J. Org. Chem.* **2021**, *86* (1), 782−793.

(7) Bortnikov, E. O.; Smith, B. S.; Volochnyuk, D. M.; Semenov, S. N. Stirring-Free Scalable Electrosynthesis Enabled by Alternating Current. *Chem. - Eur. J.* **2023**, *29* (18), No. e202203825.

(8) Zeng, L.; Jiao, Y.; Yan, W. S.; Wu, Y.; Wang, S. C.; Wang, P. J.; Wang, D.; Yang, Q. H.; Wang, J. X.; Zhang, H.; Lei, A. Asymmetric-Waveform Alternating Current-Promoted Silver Catalysis for C−H Phosphorylation. *Nat. Synth.* **2023**, *2* (2), 172−181.

(9) Wang, D.; Jiang, T.; Wan, H.; Chen, Z.; Qi, J.; Yang, A.; Huang, Z.; Yuan, Y.; Lei, A. Alternating Current Electrolysis Enabled Formal C-O/O-H Cross-Metathesis of 4-Alkoxy Anilines with Alcohols.

Angew. Chem., Int. Ed. **2022**, *61* (18), No. e202201543, DOI: 10.1002/anie.202201543.
(10) Yuan, Y.; Qi, J. C.; Wang, D. X.; Chen, Z. Y.; Wan, H.; Zhu, J. Y.; Yi, H.; Chowdhury, A. D.; Lei, A. W. Radical-Radical Cross-Coupling Assisted N-S Bond Formation Using Alternating Current Protocol. *CCS Chem.* **2022**, *4* (8), 2674−2685.
(11) Zeng, L.; Yang, Q.; Wang, J.; Wang, X.; Wang, P.; Wang, S.; Lv, S.; Muhammad, S.; Liu, Y.; Yi, H.; Lei, A. Programmed Alternating Current Optimization of Cu-Catalyzed C−H Bond Transformations. *Science* **2024**, *385* (6705), 216−223.
(12) Bu, F.; Deng, Y.; Xu, J.; Yang, D.; Li, Y.; Li, W.; Lei, A. Electrocatalytic reductive deuteration of arenes and heteroarenes. *Nature* **2024**, *634* (8034), 592−599.
(13) Kawamata, Y.; Hayashi, K.; Carlson, E.; Shaji, S.; Waldmann, D.; Simmons, B. J.; Edwards, J. T.; Zapf, C. W.; Saito, M.; Baran, P. S. Chemoselective Electrosynthesis Using Rapid Alternating Polarity. *J. Am. Chem. Soc.* **2021**, *143* (40), 16580−16588.
(14) Hayashi, K.; Griffin, J.; Harper, K. C.; Kawamata, Y.; Baran, P. S. Chemoselective (Hetero)Arene Electroreduction Enabled by Rapid Alternating Polarity. *J. Am. Chem. Soc.* **2022**, *144* (13), 5762−5768.
(15) Hioki, Y.; Costantini, M.; Griffin, J.; Harper, K. C.; Merini, M. P.; Nissl, B.; Kawamata, Y.; Baran, P. S. Overcoming the Limitations of Kolbe Coupling with Waveform-Controlled Electrosynthesis. *Science* **2023**, *380* (6640), 81−87.
(16) Garrido-Castro, A. F.; Hioki, Y.; Kusumoto, Y.; Hayashi, K.; Griffin, J.; Harper, K. C.; Kawamata, Y.; Baran, P. S. Scalable Electrochemical Decarboxylative Olefination Driven by Alternating Polarity. *Angew. Chem., Int. Ed.* **2023**, *62* (42), No. e202309157.
(17) Hibino, T.; Kobayashi, K.; Nagao, M.; Zhou, D. W.; Chen, S. Y.; Yamamoto, Y. Alternating Current Electrolysis for Individual Synthesis of Methanol and Ethane from Methane in a Thermo-electrochemical Cell. *ACS Catal.* **2023**, *13* (13), 8890−8901.
(18) He, M.; Wu, Y.; Li, R.; Wang, Y.; Liu, C.; Zhang, B. Aqueous Pulsed Electrochemistry Promotes C−N Bond Formation via a One-Pot Cascade Approach. *Nat. Commun.* **2023**, *14*, No. 5088.
(19) Zhu, S. J.; Lin, Y. C.; Yuan, G. C.; He, X.; Yu, C.; Ye, K. Y. Electrochemical Denitrative Cyclization Driven by Alternating Polarity. *Org. Lett.* **2025**, *27* (5), 1186−1191.
(20) Fors, S. A.; Yap, Y. J.; Malapit, C. A. Effect of Alternating Polarity in Electrochemical Olefin Hydrocarboxylation. *Angew. Chem., Int. Ed.* **2025**, *64* (24), No. e202424865.
(21) De Bon, F.; Fantin, M.; Pereira, V. A.; Bernardino, T. J. L.; Serra, A. C.; Matyjaszewski, K.; Coelho, J. F. J. Electrochemically Mediated Atom Transfer Radical Polymerization Driven by Alternating Current. *Angew. Chem., Int. Ed.* **2024**, *63* (29), No. e202406484.
(22) Poh, Y. R.; Kawamata, Y.; Yuen-Zhou, J. Physicochemical Principles of AC Electrosynthesis: Reversible Reactions. *J. Am. Chem. Soc.* **2024**, *146* (36), 24978−24988.
(23) Poh, Y. R.; Yuen-Zhou, J. Stirring Effects on AC-Induced Chemoselectivity in Reversible Electrochemical Reactions. *J. Phys. Chem. C* **2025**, *129* (7), 3561−3569.
(24) Li, H.; Li, Y.; Chen, J.; Lu, L.; Wang, P.; Hu, J.; Ma, R.; Gao, Y.; Yi, H.; Li, W. Scalable and Selective Electrochemical Hydrogenation of Polycyclic Arenes. *Angew. Chem., Int. Ed.* **2024**, *63* (32), No. e202407392.
(25) Liu, D.-H.; Ma, J. Recent Advances in Dearomative Partial Reduction of Benzenoid Arenes. *Angew. Chem., Int. Ed.* **2024**, *63* (21), No. e202402819.
(26) Puthongkham, P.; Venton, B. J. Recent Advances in Fast-Scan Cyclic Voltammetry. *Analyst* **2020**, *145* (4), 1087−1102.
(27) Roberts, J. G.; Sombers, L. A. Fast-Scan Cyclic Voltammetry: Chemical Sensing in the Brain and Beyond. *Anal. Chem.* **2018**, *90* (1), 490−504.

https://doi.org/10.1021/jacs.5c08873
J. Am. Chem. Soc. XXXX, XXX, XXX−XXX